Phase-Aberration Correction with a 3-D Ultrasound Scanner: Feasibility Study

Nikolas M. Ivancevich, Jeremy J. Dahl, Gregg E. Trahey, *Member, IEEE*, and Stephen W. Smith, *Member, IEEE*

***Abstract*—We tested the feasibility of using adaptive imaging, namely phase-aberration correction, with two-dimensional (2-D) arrays and real-time, 3-D ultrasound. Because of the high spatial frequency content of aberrators, 2-D arrays, which generally have smaller pitch and thus higher spatial sampling frequency, and 3-D imaging show potential to improve the performance of adaptive imaging. Phase-correction algorithms improve image quality by compensating for tissue-induced errors in beamforming. Using the illustrative example of transcranial ultrasound, we have evaluated our ability to perform adaptive imaging with a real-time, 3-D scanner. We have used a polymer casting of a human temporal bone, root-mean-square (RMS) phase variation of 45.0 ns, full-width-half-maximum (FWHM) correlation length of 3.35 mm, and an electronic aberrator, 100 ns RMS, 3.76 mm correlation, with tissue phantoms as illustrative examples of near-field, phase-screen aberrators. Using the multilag, least-squares, cross-correlation method, we have shown the ability of 3-D adaptive imaging to increase anechoic cyst identification, image brightness, contrast-to-speckle ratio (CSR), and, in 3-D color Doppler experiments, the ability to visualize flow. For a physical aberrator skull casting we saw CSR increase by 13% from 1.01 to 1.14, while the number of detectable cysts increased from 4.3 to 7.7.**

I. Introduction

Recently, researchers have applied adaptive imaging techniques, including phase-aberration correction, to 1.5D and 1.75D arrays, typically 3×80 to 6×96 elements [1]–[5]. These multirow arrays allow focusing in both azimuth and elevation dimensions and enable better estimation of aberration profiles. These methods have been shown to increase image resolution and contrast by correcting two-dimensional (2-D) aberrations in the acoustic wavefront. Acoustic wavefront aberration and errors in beam forming can originate from many different causes, though generally from tissue inhomogeneities or gross sound speed errors. These can result in amplitude and/or phase errors in received wavefronts. Aberrators can be modeled as either being distributed throughout the media, or as being a thin layer that disturbs only phase, the so-called near-field, phase-screen model [6]. The measured aberration profiles generally are characterized by their root-mean-square (RMS) amplitude (measured in nanoseconds) and their full-width-half-maximum (FWHM) autocorrelation length (measured in millimeters). Past measurements have shown breast aberrators, for example, to have a correlation length, and therefore spatial period, from 2–8 mm [1]. Thus it is imperative to adequately sample this aberrator by using a sampling (i.e., interelement spacing) of at most 1 mm. Although most 1-D transducers meet this criteria in the lateral dimension, they fall far from it in the elevation dimension. Even with 1.75D arrays, there is limited sampling in the elevation dimension, with typical elevation dimensions of 1 mm [7] to 2.5 mm [5]. Research has suggested that an elevation pitch at least 75%, but perhaps as fine as 25 to 30% of the aberration correlation length, might be needed for effective aberration measurements [2], [8].

Although there are many methods and models for estimating and correcting aberrations [6], [9]–[18], for a thin layer of subcutaneous fat or bone, the near-field phase-screen model coupled with a multilag, least-squares, correlation-based phase error algorithm has been shown to improve image quality in both 1-D and 1.75D arrays [19]. For breast and abdomen imaging, though, this might not be such a good approximation as there often are other anatomical layers or distributed inhomogeneities. Therefore, for our illustrative example, we have used transcranial scanning, especially through the temporal bone. The skull is thin in this region (approximately 1–3-mm thick) [20], it is located only at the near field of the transducer, and its speed of sound is about 2650 m/s [21], greater than the scanner's assumed speed of 1540 m/s, makes it appear even thinner than normal tissue. But for fat, speed of sound 1480 m/s, the layer appears thicker than in reality. Brain tissue has a sound speed of about 1530 m/s [22].

We have had a long-standing interest in real-time ultrasound imaging of the brain. To our knowledge, we described the first real-time B-scans of the brain in 1978 [23]. In 1986, we described a real-time adaptive scanner for transcranial ultrasound, modeling the skull as a plate of uniform thickness [24]. In 2004, we described the first real-time, 3-D images of the brain, including real-time, 3-D color Doppler images of cerebral vessels [25].

In this feasibility study, we describe the application of aberration correction algorithms to a 2-D array transducer and a real-time, 3-D ultrasound scanner developed by Duke University and Volumetrics Medical Imaging (VMI, Durham, NC) [26], [27]. After correction for an electronic aberrator and a polymer casting of the human temporal bone, we see marked improvement in identification of anechoic lesions in a tissue phantom, overall image brightness,

Manuscript received November 29, 2005; accepted March 7, 2006.

The authors are with the Department of Biomedical Engineering, Duke University, Durham, NC 27708 (e-mail: ni3@duke.edu).

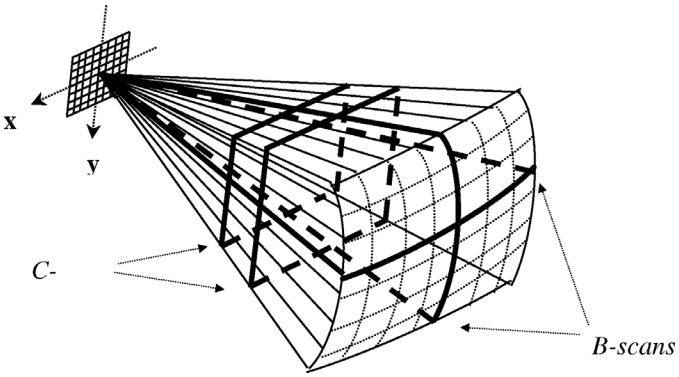

Fig. 1. The volumetrics scanner uses a 2-D matrix array to image a 65° × 65° pyramidal volume and can simultaneously display two orthogonal B-scans and two oblique C-scans.

contrast-to-speckle ratio, and the ability to visualize flow in color Doppler imaging.

II. Methods

A. Volumetrics Scanner System and Transducer

The commercial VMI ultrasound scanner generates a real-time, 3-D pyramidal scan of 65° using as many as 512 transmitters and 256 receive channels. The scanner uses 16:1 receive mode parallel processing to generate 4096 B-mode image lines at up to 30 volumes per second. Fig. 1 shows a schematic of the matrix phased-array transducer producing the pyramidal scan with two simultaneous orthogonal B-mode image planes (perpendicular to the transducer array) and two C-mode planes (parallel to the array). Alternatively, each image plane can be positioned at any desired angle and depth. By integrating and spatially filtering between two user-selected planes (e.g., the C-mode planes), the system also displays real-time, 3-D-rendered images as well as real-time, 3-D pulsed and 3-D color flow Doppler imaging.

The transcranial transducers used in this feasibility study both consisted of a $40 \times 40 = 1600$ element sparse 2-D arrays operating with 30% fractional bandwidth at 2.5 MHz and 3.5 MHz, volumetrics model numbers VL25B and VL35A, respectively, previously described by Light *et al.* 1998 [28]. The active elements of the array, shown in Fig. 2, include 440 transmit elements and 256 receive elements with a minimum interelement spacing of 0.35 mm and total aperture diameter = 13 mm.

The average element uniformity over a 4×4 group of receive elements in the center of the 2.5 MHz array was tested by pulsing a needle hydrophone (Materials Assurance, Norwich, CT) with a Panametrics Model 5073PR (Waltham, MA) pulser/receiver set to have a pulse repetition frequency (PRF) of 500 Hz, energy of 2, and damping of 1, while receiving on individual elements of the transducer. Averaged (100X) oscilloscope traces were downloaded to a computer, and the normalized covariance between nearest neighbors was found. The average nearest-neighbor element uniformity was found to be 99.3%.

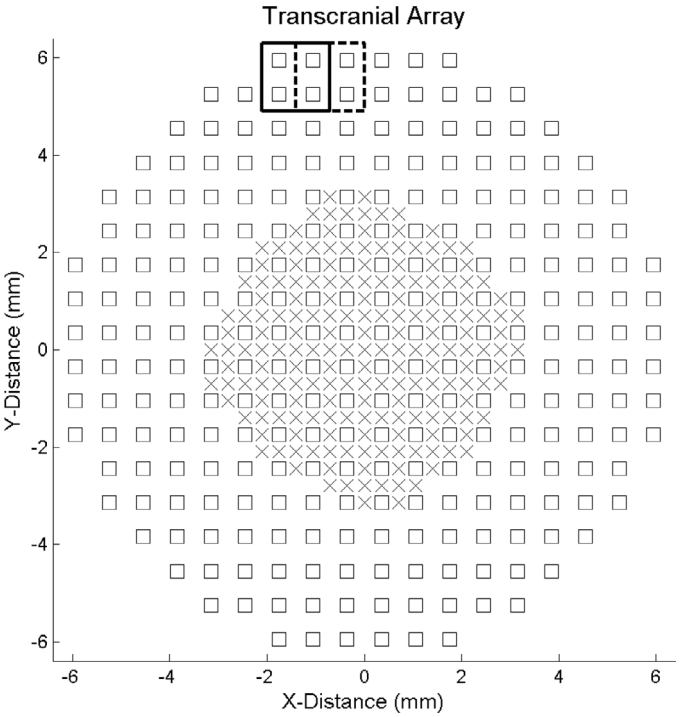

Fig. 2. Transducer layout. The periodic array used has 440 active elements. All elements transmit; the 256 square elements receive, x elements are transmit only. Solid and dashed boxes show successive positions of the aperture for RF acquisition.

The bandwidth of the transducers when attached to the system was found by imaging the tip of a wire target (0.55 mm diameter) in a water tank and acquiring the radio frequency (RF) signal from the scanner, shown in Fig. 3. The −6 dB fractional bandwidth, also shown in Fig. 3, was found to be 30%.

B. Data Acquisition

To acquire the raw RF speckle data for aberration correction, we focused the 440 transmit elements at 4 cm or 7 cm down the center of the 3-D scan (0° azimuth, 0° elevation) in a tissue phantom while receiving on an aperture of 2×2 elements, highlighted in the solid box in Fig. 2. A schematic of the dataflow is shown in Fig. 4. The 2×2 aperture is stepped across the entire receive aperture with every new transmit pulse, as illustrated by the dashed box in Fig. 2. This results in 221 RF data lines sampled at 0.7 mm spacing on the transducer aperture. The RF data is amplified using the Panametrics amplifier and sent to a Signatec PDA12 waveform digitizer (Corona, CA) installed in a Dell computer. The digitizer acquires a 1.6 cm long echo centered about the focus at 7 cm and sampled at 25 MHz. The digitizer has 2 MB of onboard memory, and thus has sufficient space to capture multiple series of these 221 lines and average them for increased signal-to-noise ratio (SNR); we found that 15 averages gave an SNR sufficiently high for correction. The data then is read by

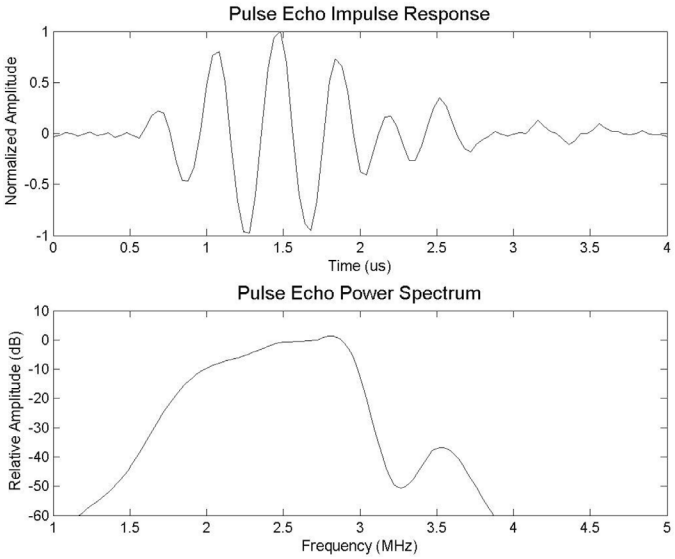

Fig. 3. Pulse-echo impulse response of 2.5 MHz transducer in time and frequency domains.

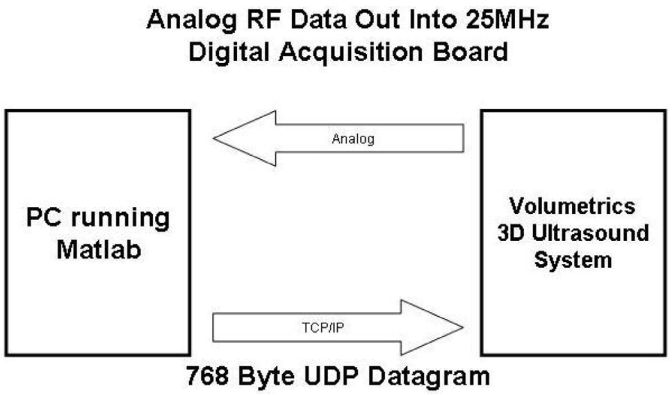

Fig. 4. Dataflow. The volumetrics system outputs analog RF data to a computer, which after calculating phase-shifts, sends these data back via a TCP/IP connection.

MATLAB (The MathWorks, Natick, MA) and manipulated there.

C. Phantoms and Aberrators

The electronic aberrator used was a profile from a polymer casting of the human temporal bone we measured by transmitting on single elements, receiving on a needle hydrophone, and using the linear multilag, least-squares, cross-correlation method detailed below to compute time shifts [1], [6], [11]. The RMS of the aberration was 101 ns with an average autocorrelation width of 3.76 mm. For physical aberrators, we used the same skull casting and placed it between the transducer and the phantom of interest. To evaluate image brightness and CSR, we used a Gammex RMI (Middleton, WI) model 408 spherical cyst phantom with anechoic spheres of 4 mm diameter, contrast = −35 dB, as a test object. For evaluation of Doppler performance, we used an ATS Laboratories (Bridgeport, CT) model 523A Doppler phantom with a 2 mm vessel. A 10 g/l mixture of cornstarch in water flowed, gravity fed, at a constant rate through the tubing while scanning.

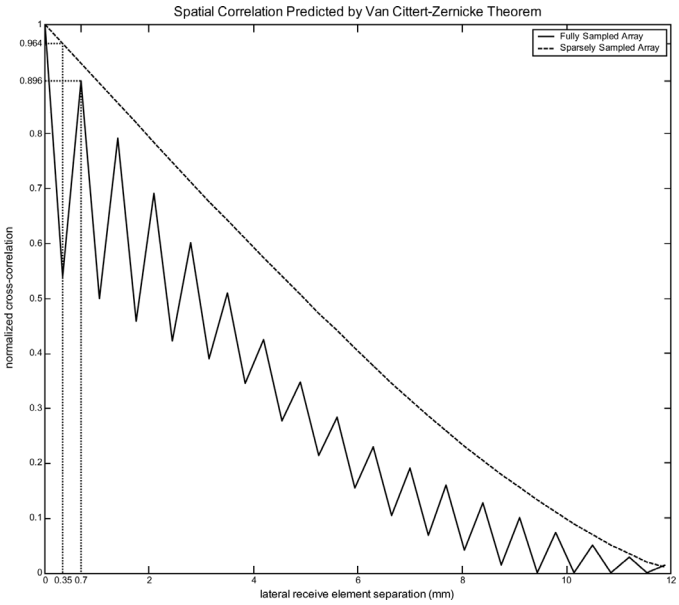

Fig. 5. The correlation between speckle signals is shown as a function of spacing for our periodic array (solid line) and for a fully sampled array of the same footprint (dashed line). The dotted line shows the value for adjacent receive elements on the array.

D. Cramer-Rao Lower Bound Measurements

The Cramer-Rao lower bound describes a lower-bound for correlation-based, time-delay estimators [29]. It is especially useful to both predict the performance of a phase-correction scheme and compare the performance of various schemes [30]. Integral to the calculation of the Cramer-Rao lower bound, or jitter, is the determination of the spatial correlation of the aperture. The Van Cittert-Zernicke theorem states that, for an incoherent, diffuse source, the receive spatial correlation function is equal to the Fourier transform of the intensity pattern of the incoherent source [31], [32]. Therefore, the mutual coherence, Γ_{AB}, of two stationary signals A and B located at x_1 and x_2 can be described by:

$$\Gamma_{AB}(x_1, x_2) = R_{TT}(x_1 - x_2), \tag{1}$$

where R_{TT} is the autocorrelation of the transmit aperture. This value declines with aberration present. In Fig. 5, we see the autocorrelations of both the transmit aperture for our periodic array (solid line) and for a fully sampled array of the same footprint (dotted line), which, therefore, gives us the maximum correlation value for lines of speckle data as a function of separation between receive apertures. Thus for our periodic array, the correlation of adjacent receive elements is 89.6%, and for a fully sampled array, the correlation of adjacent receive elements increases to 96.4%. Using our 2×2 geometry, we calculate a theoretical correlation of 95.4% for half-overlapping apertures.

As an experimental check of the Van Cittert-Zernicke prediction, we acquired 10 sets of unaberrated speckle data from the tissue-mimicking phantom and calculated the maximum correlation between nearest neighbors, yielding an average value of 83.8 ± 4.1%, which is in reasonable agreement with the predicted 95.4% above.

The Cramer-Rao lower bound shows the jitter of a correlation-based, time-delay estimator to be:

$$\tau \leq \sqrt{\frac{3}{2f_0^3\pi^2\left(B^3+12B\right)}\left(\frac{1}{\rho^2}\left(1+\frac{1}{\mathrm{SNR}^2}\right)^2-1\right)}, \quad (2)$$

where τ is the jitter, f_0 is the array center frequency, B is the -6 dB fractional bandwidth, ρ is the correlation coefficient between two signals, and SNR is the signal-to-noise ratio of the data [29]. We computed the correlation coefficient between subsequent measurements taken from the same 2×2 element receive aperture for an average of 97.8%. It can be shown, using the definitions of SNR and the correlation coefficient, that for a zero-mean process [33]:

$$\mathrm{SNR} = \frac{1}{\sqrt{1-\rho^2}}. \quad (3)$$

Using the measured correlation and (3), we computed a SNR of 13.5 dB. Using our experimental results and (2), we calculated a lower bound of the jitter of 19.3 ns for our aberration measurements with the 2.5 MHz array.

E. Aberration Estimation

A linear, multilag, least-squares cross-correlation method was used to estimate the aberration profile [1], [6], [11]. In this algorithm, time-delay estimates are calculated for four nearest neighbors, two in both azimuth and elevation. Calculation of time-delay estimates in this manner yields an over-determined system of equations for which least-mean-squares will provide the best fit aberration profile that enforces phase closure. Using this method, time-shift estimates, vector T, are found by using the equation:

$$T = \left(M^T M\right)^{-1} M^T D, \quad (4)$$

where D is a vector comprised of the differential time shift between elements, and M is the 409×221 model matrix, which specifies how the arrival times are related to time estimates between element pairs. This process yields 221 time shifts, $\Delta\tau$, for each group of four receive elements. This map of time shifts then is interpolated to yield the shift at each receive and transmit element in Fig. 2, then converted into system clock cycles (25 ns increments) for a total of 768 shifts.

F. Data Transfer

To send the time shifts back to the scanner, we encode the 768 $\Delta\tau$'s as 1 byte numbers and send them to the scanner as a UDP datagram via a TCP/IP transfer over a 10 baseT Ethernet connection. The scanner, upon receiving these shifts, runs a subroutine to update the system delays. For transmit, there are 2^{19} delays [512 elements × 256 lines × 4 modes (B-mode, M-mode, 3-D pulse Doppler, and 3-D color flow Doppler)]. For receive there are 2^{24} delays (256 elements × 256 lines × 16:1 parallel processing lines × 10 focal zones). Updating these delays on the 100 MHz clock and transferring the delays to the receive processor boards takes about 25 seconds. Once all the delays are updated, the system resumes scanning. The whole process takes 1 minute.

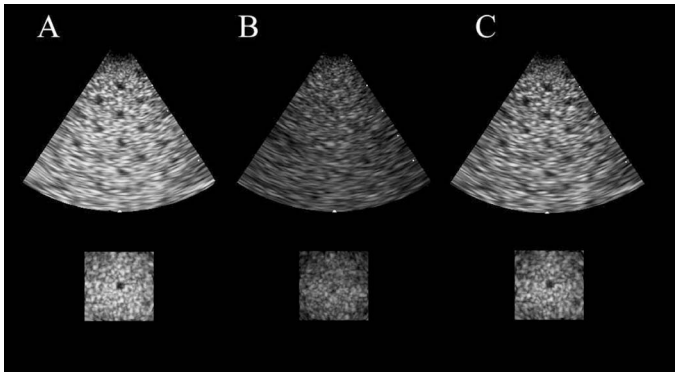

Fig. 6. Electronic aberrator. Simultaneous orthogonal B-mode and C-mode image planes from 3-D scans of the RMI 408 tissue phantom with 4 mm spherical anechoic lesions. The figure compares the control (A), aberrated (B), and phase-corrected (C) images.

III. Results

A. Electronic Aberrator

Fig. 6 shows control (A), aberrated (B), and corrected (C), results from an electronic aberrator experiment performed at a constant gain setting. The electronic aberrator's delays were applied to both transmit and receive delays in the beamformer of the volumetrics scanner, resulting in the image in Fig. 6(B). After an estimate of the aberration profile was made using the process detailed above, these measured delays were subtracted from the applied delays to leave a residual aberrator. These residual delays were applied to the RF through the system's beamformer to produce a corrected scan. This process was repeated three times, until the image quality stabilized. This residual aberrator was RMS 52 ns with a 2.4-mm correlation length. The final corrected image is shown in Fig. 6(C). To evaluate the performance of the correction on image quality, we used three metrics: number of detectable cysts, average speckle brightness (mean pixel value at a given depth), and CSR defined as:

$$\mathrm{CSR} = \frac{\left|\langle S_{\mathrm{speckle}}\rangle - \langle S_{\mathrm{cyst}}\rangle\right|}{\sqrt{\sigma^2_{\mathrm{speckle}} + \sigma^2_{\mathrm{cyst}}}}, \quad (5)$$

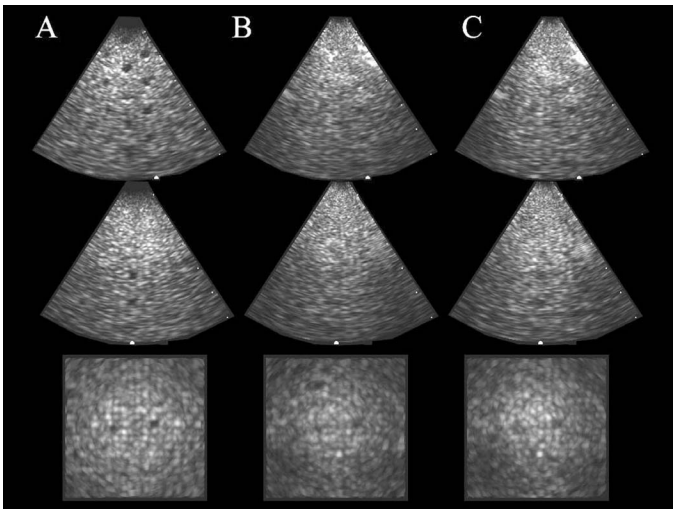

Fig. 7. Physical aberrator. Simultaneous orthogonal B-mode and C-mode image planes from 3-D scans of the RMI 408 tissue phantom with 4-mm spherical anechoic lesions. The figure compares the control (A), aberrated (B), and phase corrected (C) images for a skull cast aberrator.

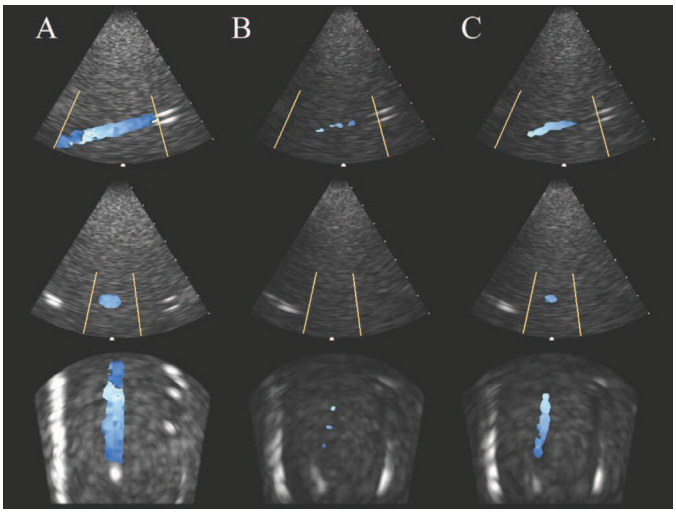

Fig. 8. Physical aberrator Doppler correction. The columns show control (A), aberrated (B), and corrected (C) images of a 2-mm vessel with constant flow. The rows show the scanner's three orthogonal images. Images were taken with constant B-mode and color gain settings.

where S_{cyst} and S_{speckle} are the signals in a cyst and in a adjacent area of speckle, and σ^2 denotes the variance of the subscripted signal [34], [35]. The average numbers of cysts present in the three orthogonal images, as judged by three independent observers, are 14 in the control, 4 in the aberrated, and 14 in the corrected. The average brightness increased in the corrected scan by 41%, returning to 77% of its original value. The CSR calculated from the cysts, which all observers detected, increased from 0.87 ± 0.06 to 1.33 ± 0.23, matching the control value of 1.29 ± 0.37.

B. Physical Aberrator

In Fig. 7, we show the results of a phase-aberration correction on a piece of polymer casting of a human temporal bone with a 3.5 MHz transducer. The attenuation of the casting prevents us from leaving the gain constant between images; when the aberrated case is sufficiently bright, the control is saturated. Thus we adjusted gain to maximize perceived quality in each image. We measured the aberrator to have an RMS phase-shift of 45.0 ns and a correlation length of 3.35 mm. Again, the average number of cysts detected by three independent observers and CSR were used as image quality metrics. In the control B-scans, Fig. 7(A), on average 14.3 cysts are detected, compared to 4.3 in the aberrated image, Fig. 7(B), and 7.7 in the corrected image, Fig. 7(C). For the cysts identified by all three observers, the CSR increased from 1.01 ± 0.52 in the aberrated to 1.14 ± 0.17 in the corrected, a return to 79% of its original value of 1.45 ± 0.45.

C. Doppler Imaging

To simulate images of cerebral vessels, in Fig. 8 we show the results of a correction with the skull cast physical aberrator, RMS strength 39.4 ns and correlation length 3.10 mm, of blood-flow in a phantom at 2.5 MHz. The three rows are orthogonal scans of the blood vessel, one short-axis B-scan, one long-axis B-scan, and a C-scan long-axis view, selected from the real-time, 3-D scan. Unlike the last experiment, the B-mode and color gains remained constant throughout these images. The tissue speckle brightness increased by 10.8% from the aberrated to the corrected image. There also is a large improvement in Doppler signal. In both the control and the corrected images the vessel is fully covered in color Doppler signal; and in the aberrated image, it is difficult to distinguish between the signal in the vessel and electronic noise. Because of the variability of the frames in this experiment—most likely due to air bubbles and/or clumps of cornstarch—we used the scanner's persistence mode (exponentially weighted temporal averaging) to temporally smooth the images.

IV. Discussion

A. Challenges to High-Speed Phase Correction

For this system of 3-D ultrasound, phase-aberration correction to be a useful high-speed option, several obstacles still must be overcome. Currently, each correction takes 1 minute, though we can reduce this at each step of the correction process: transmission and RF acquisition, phase-lag computation, data transfer, and delay updating. Only our need for 15× averaging imposes a fundamental limit on our correction time; assuming an image depth of 15 cm, this takes 380 ms. If, however, we could access the digital echo data within the scanner, we would have less noise, allowing us to lower our number of full transmits from 15 to

TABLE I
IMAGE QUALITY METRICS FOR ELECTRONIC AND PHYSICAL ABERRATION CORRECTIONS.

	Aberrator strength	No. of Cysts Detected			CSR		
		Control	Aberrated	Corrected	Control	Aberrated	Corrected
Electronic aberrator	52.0 ns, 2.4 mm	14	4	14	1.29 ± 0.37	0.87 ± 0.06	1.33 ± 0.23
Physical aberrator	45.0 ns, 3.34 mm	14.3	4.3	7.7	1.45 ± 0.45	1.01 ± 0.52	1.14 ± 0.17

perhaps 1, and using the 16:1 receive parallel processing, we would be able to acquire data in groups of 16, lowering our number of transmit lines to 16, which would shorten this step's time to just 1 ms [36]. We also plan to try using a different algorithm to compute phase lags, such as the speckle brightness technique [14], and to streamline the code by translating all MATLAB code to C++, and through this we could approach the phase-aberration correction times reported by McAleavey *et al.* [37] of 1.4 s and of Rigby *et al.* [5] of 350 ms.

B. Dedicated Transcranial Transducer

Currently we are using commercial transthoracic arrays to image transcranially, but there would be significant advantages to using a dedicated array designed specifically for this function. After finding the typical correlation lengths for skull samples, we could make sure that our spatial frequency (i.e., interelement spacing) is high enough to adequately sample the aberration profiles typically encountered. Also, by designing a more fully sampled array, we would not only increase the maximum correlation between signals dictated by the Van Cittert-Zernicke toward the fully sampled array's value of 96.4% shown in Fig. 5, but also increase the spatial sampling frequency of the array. Raising this value would increase the maximum normalized covariance of our signals, ρ, and thus lead to lower jitter error as dictated by the Cramer-Rao lower bound.

C. Isoplanatic Patch

The near-field, phase-screen aberration model assumes an infinitesimally thin aberrating layer at the face of the transducer. Clearly, in our example, although the layer is thin, it does have a thickness (2–3 mm). This means that the measurement of the aberration will be valid only over a certain angular region, the so-called isoplanatic patch. Measurements of the size of this patch have been performed in abdominal [38], breast, liver, and thyroid tissue [7]. From a crude preliminary experiment, we measured an isoplanatic patch of roughly $\pm 10^\circ$ for our skull casting. We plan on making further measurements of the isoplanatic patch, and we have developed a system for measuring four aberrations spaced 10 degrees apart and applying them to quadrants of transmit/receive lines.

V. CONCLUSIONS

In this paper, we have shown our ability to use phase-aberration correction techniques to increase image quality in simulated transcranial ultrasound imaging. The image quality in electronic and physical aberrator experiments has shown a dramatic increase as measured by cyst identification, brightness, and CSR (results summarized in Table I). We also have shown that 3-D transcranial Doppler imaging can be significantly improved with adaptive imaging. We also have demonstrated that our illustrative example of the human temporal bone can be modeled well as a near-field, phase-screen aberrator. Given our average measured correlation lengths, it also is a setting for which a small pitch 2-D array is necessary; our spatial sampling period of 0.7 mm is fine enough to meet the Nyquist criterion when measuring skull aberrators. Thus for future work, we plan to further investigate transcranial ultrasound as a candidate for 3-D phase-aberration correction.

REFERENCES

[1] R. C. Gauss, G. Trahey, and M. S. Soo, "Wavefront estimation in the human breast," *Proc. SPIE*, vol. 4325, pp. 172–181, 2001.
[2] J. Lacefield and R. Waag, "Time-shift estimation and focusing through distributed aberration using multirow arrays," *IEEE Trans. Ultrason., Ferroelect., Freq. Contr.*, vol. 48, pp. 1606–1624, 2001.
[3] Y. Li and B. Robinson, "Phase aberration correction using near-field redundancy—Two-dimensional array algorithm," in *Proc. IEEE Ultrason. Symp.*, 2000, pp. 1729–1733.
[4] D. Liu and R. Waag, "A comparison of ultrasonic wavefront distortion and compensation in one-dimensional and two-dimensional apertures," *IEEE Trans. Ultrason., Ferroelect., Freq. Contr.*, vol. 42, pp. 726–733, 1995.
[5] K. W. Rigby, C. L. Chalek, B. H. Haider, R. S. Lewandowski, M. O'Donnell, L. S. Smith, and D. G. Wildes, "Improved in vivo abdominal image quality using real-time estimation and correction of wavefront arrival time errors," presented at *Proc. IEEE Ultrason. Symp.*, 2000, San Juan, P.R.
[6] S. W. Flax and M. O'Donnell, "Phase-aberration correction using signals from point reflectors and diffuse scatterers: Basic principles," *IEEE Trans. Ultrason., Ferroelect., Freq. Contr.*, vol. 35, pp. 758–767, 1988.
[7] J. J. Dahl, M. S. Soo, and G. E. Trahey, "Spatial and temporal aberrator stability for real-time adaptive imaging," *IEEE Trans. Ultrason., Ferroelect., Freq. Contr.*, vol. 52, pp. 1504–1517, 2005.
[8] J. Lacefield and R. Waag, "Effect of transmit focus characteristics on estimates of aberration," in *Proc. IEEE Ultrason. Symp.*, 2000, pp. 1665–1668.
[9] G. C. Ng, S. S. Worrell, P. D. Freiburger, and G. E. Trahey, "A comparative evaluation of several algorithms for phase aberration correction," *IEEE Trans. Ultrason., Ferroelect., Freq. Contr.*, vol. 41, pp. 631–643, 1994.
[10] D. L. Liu and R. C. Waag, "Correction of ultrasonic wavefront distortion using backpropagation and a reference waveform

method for time-shift compensation," *J. Acoust. Soc. Amer.*, vol. 96, pp. 542–555, 1994.

[11] D. Liu and R. Waag, "Time-shift compensation of ultrasonic pulse focus degradation using least-mean-square error-estimates of arrival time," *J. Acoust. Soc. Amer.*, vol. 95, pp. 542–555, 1994.

[12] M. Fink, "Time reversal of ultrasonic fields—Part I: Basic principles," *IEEE Trans. Ultrason., Ferroelect., Freq. Contr.*, vol. 39, pp. 555–566, 1992.

[13] D. Rachlin, "Direct estimation of aberrating delays in pulse-echo imaging systems," *J. Acoust. Soc. Amer.*, vol. 88, pp. 191–198, 1990.

[14] L. Nock, G. E. Trahey, and S. W. Smith, "Phase aberration correction in medical ultrasound using speckle brightness as a quality factor," *J. Acoust. Soc. Amer.*, vol. 85, pp. 1819–1833, 1989.

[15] Y. Li, "Phase aberration correction using near-field signal redundancy—Part I: Principles," *IEEE Trans. Ultrason., Ferroelect., Freq. Contr.*, vol. 44, pp. 355–371, 1997.

[16] F. Lin and R. C. Waag, "Estimation and compensation of ultrasonic wavefront distortion using a blind system identification method," *IEEE Trans. Ultrason., Ferroelect., Freq. Contr.*, vol. 49, pp. 739–755, 2002.

[17] K. Hynynen and J. Sun, "Trans-skull ultrasound therapy: The feasibility of using image-derived skull thickness information to correct the phase distortion," *IEEE Trans. Ultrason., Ferroelect., Freq. Contr.*, vol. 46, pp. 752–765, 1999.

[18] J. White, G. T. Clement, and K. Hynynen, "Transcranial ultrasound focus reconstruction with phase and amplitude correction," *IEEE Trans. Ultrason., Ferroelect., Freq. Contr.*, vol. 52, pp. 1518–1522, 2005.

[19] A. Fernandez, K. Gammelmark, J. Dahl, C. Keen, R. Gauss, and G. Trahey, "Synthetic elevation beamforming and image acquisition capabilities using an 8×128 1.75D array," *IEEE Trans. Ultrason., Ferroelect., Freq. Contr.*, vol. 50, pp. 40–57, 2003.

[20] U. Bogdahn, G. Becker, and F. Schlachetzki, *Echoenhancers and Transcranial Color Duplex Sonography.* Berlin: Blackwell Science, 1998.

[21] F. J. Fry and J. E. Barger, "Acoustic properties of the human skull," *J. Acoust. Soc. Amer.*, vol. 63, pp. 1576–1590, 1978.

[22] S. A. Goss, R. L. Johnston, and F. Dunn, "Comprehensive compilation of empirical ultrasonic properties of mammalian tissues," *J. Acoust. Soc. Amer.*, vol. 64, pp. 423–457, 1978.

[23] S. W. Smith, O. T. von Ramm, J. A. Kisslo, and F. L. Thurstone, "Real time ultrasound tomography of the adult brain," *Stroke*, vol. 9, pp. 117–122, 1978.

[24] S. W. Smith, G. E. Trahey, and O. T. von Ramm, "Phased array ultrasound imaging through planar tissue layers," *Ultrasound Med. Biol.*, vol. 12, pp. 229–243, 1986.

[25] S. W. Smith, K. Chu, S. F. Idriss, N. M. Ivancevich, E. D. Light, and P. D. Wolf, "Feasibility study: Real-time 3-D ultrasound imaging of the brain," *Ultrasound Med. Biol.*, vol. 30, pp. 1365–1371, 2004.

[26] S. Smith, H. Pavy, and O. VonRamm, "High-speed ultrasound volumetric imaging-system. 1. Transducer design and beam steering," *IEEE Trans. Ultrason., Ferroelect., Freq. Contr.*, vol. 38, pp. 100–108, 1991.

[27] O. VonRamm, S. Smith, and H. Pavy, "High-speed ultrasound volumetric imaging-system. 2. Parallel processing and image display," *IEEE Trans. Ultrason., Ferroelect., Freq. Contr.*, vol. 38, pp. 109–115, 1991.

[28] E. Light, R. Davidsen, J. Fiering, T. Hruschka, and S. Smith, "Progress in two-dimensional arrays for real-time volumetric imaging," *Ultrason. Imag.*, vol. 20, pp. 1–15, 1998.

[29] W. F. Walker and G. E. Trahey, "A fundamental limit on the performance of correlation based phase correction and flow estimation techniques," *IEEE Trans. Ultrason., Ferroelect., Freq. Contr.*, vol. 41, pp. 644–654, 1994.

[30] F. Viola and W. F. Walker, "A comparison of the performance of time-delay estimators in medical ultrasound," *IEEE Trans. Ultrason., Ferroelect., Freq. Contr.*, vol. 50, pp. 392–401, 2003.

[31] D. L. Liu and R. C. Waag, "About the application of the Van Cittert-Zernicke theorem in ultrasonic imaging," *IEEE Trans. Ultrason., Ferroelect., Freq. Contr.*, vol. 42, pp. 590–601, 1995.

[32] R. Mallart and M. Fink, "The Van Cittert-Zernicke theorem in pulse echo measurements," *J. Acoust. Soc. Amer.*, vol. 90, pp. 2718–2727, 1991.

[33] E. Parzen, *Modern Probability Theory and Its Applications.* New York: Wiley, 1960.

[34] M. S. Patterson and F. S. Foster, "The improvement and quantitative assessment of B-mode images produced by an annular array cone hybrid," *Ultrason. Imag.*, vol. 5, pp. 195–213, 1983.

[35] P. C. Li and M. O'Donnell, "Improved detectability with blocked element compensation," *Ultrason. Imag.*, vol. 16, pp. 1–18, 1994.

[36] P. D. Freiburger and G. E. Trahey, "Parallel processing techniques for the speckle brightness phase aberration correction algorithm," *IEEE Trans. Ultrason., Ferroelect., Freq. Contr.*, vol. 44, pp. 431–444, 1997.

[37] S. A. McAleavey, J. J. Dahl, G. F. Pinton, and G. E. Trahey, "Real time adaptive imaging with 1.75D, high frequency arrays," in *Proc. IEEE Ultrason. Symp.*, 2003, pp. 335–338.

[38] D. L. Liu and R. C. Waag, "Estimation and correction of ultrasound wavefront distortion using pulse-echo data received in a two-dimensional aperture," *IEEE Trans. Ultrason., Ferroelect., Freq. Contr.*, vol. 45, pp. 473–490, 1998.

Nikolas M. Ivancevich was born in Evanston, IL, in 1981. He received the B.A. degree in physics (summa cum laude) from Wabash College, Crawfordsville, IN, in 2003.

Currently, he is a biomedical engineering doctoral candidate at Duke University, Durham, NC. His current research focuses on adaptive ultrasonic imaging systems for real-time volumetric imaging.

Jeremy J. Dahl was born in Ontonagon, MI, in 1976. He received the B.S. degree in electrical engineering from the University of Cincinnati, Cincinnati, OH, in 1999. He received the Ph.D. degree in biomedical engineering from Duke University, Durham, NC, in 2004. He is currently a Research Associate with the Department of Biomedical Engineering at Duke University. He is currently researching adaptive ultrasonic imaging systems and radiation force imaging methods.

Gregg E. Trahey (S'83–M'85) received the B.G.S. and M.S. degrees from the University of Michigan, Ann Arbor, MI, in 1975 and 1979, respectively. He received the Ph.D. degree in Biomedical Engineering in 1985 from Duke University, Durham, NC. He served in the Peace Corps from 1975 to 1978 and was a project engineer at the Emergency Care Research Institute in Plymouth Meeting, PA, from 1980–1982. He currently is a Professor with the Department of Biomedical Engineering at Duke University and holds a secondary appointment with the Department of Radiology at the Duke University Medical Center. He is conducting research in adaptive phase correction, radiation force imaging methods, and 2-D flow imaging in medical ultrasound.

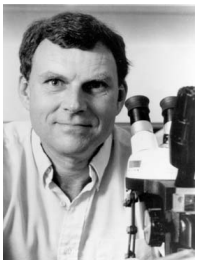

Stephen W. Smith (M'91) was born in Covington, KY, on July 27, 1947. He received the B.A. degree in physics (summa cum laude) in 1967 from Thomas More College, Ft. Mitchell, KY, the M.S. degree in physics in 1969 from Iowa State University, Ames, and the Ph.D. degree in biomedical engineering in 1975 from Duke University, Durham, NC.

In 1969, he became a Commissioned Officer in the U.S. Public Health Service, assigned to the Food and Drug Administration, Center for Devices and Radiological Health, Rockville, MD, where he worked until 1990 in the study of medical imaging, particularly diagnostic ultrasound and in the development of performance standards for such equipment. In 1978, he became an adjunct associate professor of radiology at Duke University Medical Center. In 1990, he became an associate professor of biomedical engineering and radiology, and Director of Undergraduate Studies in Biomedical Engineering at Duke University. He holds 16 patents in medical ultrasound and has authored 100+ publications in the field.

Dr. Smith is cofounder of Volumetrics Medical Imaging. He has served on the education committee of the American Institute of Ultrasound in Medicine, the executive board of the American Registry of Diagnostic Medical Sonographers, the editorial board of *Ultrasonic Imaging*, and the Technical Program Committee of IEEE-UFFC. He was corecipient of the American Institute of Ultrasound in Medicine Matzuk Award in 1988 and 1990 and corecipient of the IEEE-UFFC Outstanding Paper Award in 1983 and 1994.